Progress in Natural Science: Materials International 30 (2020) 764–774

Contents lists available at ScienceDirect

Progress in Natural Science: Materials International

journal homepage: www.elsevier.com/locate/pnsmi

Review

Electrolyte materials for intermediate-temperature solid oxide fuel cells

Huangang Shi [a,b], Chao Su [b,c], Ran Ran [d], Jiafeng Cao [b,e], Zongping Shao [b,d,*]

[a] School of Environmental Engineering, Nanjing Institute of Technology, Nanjing, 211167, China
[b] WA School of Mines, Minerals, Energy and Chemical Engineering (WASM-MECE), Curtin University, Perth, WA, 6102, Australia
[c] School of Energy and Power, Jiangsu University of Science and Technology, Zhenjiang, 212100, China
[d] State Key Laboratory of Materials-Oriented Chemical Engineering, College of Chemical Engineering, Nanjing Tech University, Nanjing, 211816, China
[e] School of Mathematics and Physics, Anhui University of Technology, Maanshan, 243032, China

ARTICLE INFO

Keywords:
Solid oxide fuel cell
Electrolyte
Oxygen ion-conducting
Proton-conducting
Dual ion-conducting

ABSTRACT

Solid oxide fuel cells (SOFCs) directly convert chemical energy that is stored in a wide range of fuels into direct current electricity, with high efficiency and low emissions, via a series of electrochemical reactions at elevated operating temperatures (generally 400–1000 °C). During such an energy conversion process, the properties of electrolyte materials determine the working principle and operating temperature of the SOFC. When considering the cost and stability, lowering the operating temperature is critical, and this has become one of the developing trends in SOFC research. The key point for realizing a reduction in operating temperature is to maintain low ohmic resistance of the electrolyte and low polarization resistance of the electrodes. In practice, the mechanical and chemical stability of the electrolyte is also a big concern. According to their differences in ion conduction mechanisms, there are three main types of electrolyte material available, namely, oxygen ion-conducting, proton-conducting, and dual ion-conducting electrolytes. In this review, we give a comprehensive summary of the recent advances in the development of these three types of electrolyte material for intermediate-temperature SOFCs. Both conductivity and stability are emphasized. In conclusion, the current challenges and future development prospects are discussed.

1. Introduction

With the rapid progress of our civilization and the exponential growth of world population, mankind's demand for energy is expanding at a high rate. During the recent past, fossil fuels have been the major energy sources and their utilization has been based mainly on combustion technology. However, its excessive and inefficient use has led to the production of huge amounts of CO_2 and impurities (SO_2, NO_x), causing major concerns about environmental pollution and climate change, which are detrimental to the healthy development of our society. For a sustainable future, renewable energy and green energy conversion/utilization technologies are urgently needed [1,2]. Fuel cells offer advanced energy conversion technology that exhibits high efficiency and low emission of environmental pollutants and greenhouse gases. There are many types of fuel cell based on different electrolyte materials. Among these, only proton-exchange membrane fuel cells (PEMFCs) and solid oxide fuel cells (SOFCs) are entirely solid-state structures, which are free from the problem of electrolyte leakage. PEMFCs usually operate at room temperature and up to 80 °C, with the advantage of a quick start that makes them suitable as the power source for electric vehicles. However, due to their low operation temperature, precious metal electrocatalysts (such as Pt) are needed, which greatly increases the cost. In addition, pure hydrogen is the necessary fuel. Unlike PEMFCs, the operating temperature of an SOFC is much higher, typically between 400 and 1000 °C. Such elevated operational temperatures effectively accelerate the electrode reaction kinetics; thus no precious metals are needed for the electrocatalysts. Thanks to the higher operating temperature, SOFCs also have the advantage of fuel flexibility. In addition to fossil fuels, renewable biomass can also be applied as the fuel source [3–5]. Therefore, SOFCs are believed to be one of the most promising fuel cells for widespread applications in the near future.

A typical SOFC single cell is composed of a porous oxide-based cathode, a dense ceramic electrolyte and a porous ceramic-metal composite anode. They form a sandwich-type structure with the electrolyte in the middle. Unlike conventional chemical redox reactions, the oxidants and reducing agents in SOFC reactions are not in direct contact. The fuel undergoes an electrochemical oxidation reaction at the anode and emits electrons that reach the cathode through an external circuit to

* Corresponding author.
E-mail addresses: zongping.shao@curtin.edu.au, shaozp@njtech.edu.cn (Z. Shao).

https://doi.org/10.1016/j.pnsc.2020.09.003
Received 2 September 2020; Received in revised form 7 September 2020; Accepted 10 September 2020
Available online 4 October 2020

enable participation in the electrochemical oxygen reduction reaction (ORR). Oxygen ions or protons transfer to the other side of the fuel cell (anode for O^{2-} and cathode for H^{+}) through the bulk of solid electrolyte to complete the final reaction. As a key part of an SOFC, the electrolyte performs several important roles. Firstly, it acts as a physical block to avoid the direct mixing of fuel and oxidant, thus the electrolyte should be fully densified, without pinholes. Secondly, the electrolyte is also an electron diffusion block to force electron transport only through the external circuit. This suggests that the electrolyte should be an electronic insulator (pure ionic conductor). Thirdly, the electrolyte also performs as a substrate for the support of both electrodes, suggesting that the mechano-thermal properties of the electrolyte and the electrodes should be well matched [6,7]. In an SOFC, the properties of the electrolyte determine the path of the reactions, the open circuit voltage, stability, mechanical performance, and operating temperature of the whole cell. Since the electrolyte faces the atmospheres of both anode and cathode, it should possess high chemical stability over a wide range of oxygen partial pressures.

The state-of-the-art SOFCs are composed of Y_2O_3 stabilized ZrO_2 (YSZ) electrolyte, Ni + YSZ cermet anode and $La_{0.8}Sr_{0.2}MnO_3$ (LSM) perovskite oxide cathode, which are usually operated at higher than 800 °C to achieve favorable power output. Nowadays, it is generally accepted that a reduction in operating temperature to the intermediate range of 400–800 °C is the key for accelerating the widespread application of SOFCs. Since the power output of an SOFC is closely related to electrode polarization resistance and electrolyte ohmic resistance, both should be kept at a sufficiently low level to ensure a high power output at reduced temperature. However, YSZ and LSM respectively show low oxygen-ion conductivity and poor catalytic activity for ORR at intermediate temperature (IT). Consequently, the state-of-the-art SOFC with thick YSZ electrolyte and LSM cathode demonstrates poor power output at temperatures lower than 800 °C [8,9]. Instead, a new cathode and electrolyte should be developed to meet the requirement of favorable power output at intermediate temperatures. During the past, considerable research activities have been directed towards the development of new cathode materials and electrolyte for intermediate temperature SOFCs (IT-SOFCs) [10–12]. Many review papers are available in the literature concerning recent advances in cathodes for IT-SOFCs, while less attention has been paid to the electrolyte [13–15]. In this review, we specifically summarize recent advances in the development of new electrolytes for IT-SOFCs. Finally, the current challenges and future development trends are provided.

2. Electrolyte materials for IT-SOFCs

In a typical SOFC, the electrolyte is interposed between the porous anode and the porous cathode, which performs one important function: to separate the anode and cathode gases. In order to satisfy this requirement, the continuity and compactness of the electrolyte layer is crucial. At the same time, the electrolyte also transfers ions between the anode and the cathode to complete the reaction of the SOFC. The ionic conduction inside the electrolyte is thus of enormous significance because it partially determines the performance of the SOFC. Depending on the different transport species, SOFCs can be generally classified as an oxygen ion-conducting SOFC (O–SOFC) or a proton-conducting SOFC (P–SOFC). Typically, proton diffusion has lower activation energy than oxygen ion diffusion. Therefore, in principle, it is easier to achieve higher conductivity for protons than oxygen ions at the lower-to-intermediate temperature range. Interestingly, another category of SOFC, called a dual ion-conducting SOFC (D-SOFC), has attracted considerable attention recently. In this cell, the electrolyte permits simultaneous diffusion of both oxygen ions and protons. Such fuel cells may enable the advantages of both O–SOFCs and P–SOFCs. As schematically displayed in Fig. 1, due to the different ion conduction mechanisms in the electrolyte, the reaction pathways of different types of SOFCs are different. As an example, taking hydrogen as the fuel and oxygen as the oxidant, the complete reaction of the three SOFCs is as follows:

$$2H_2 + O_2 \rightarrow 2H_2O \quad (1)$$

H_2 is oxidized at the anode and emits electrons, as shown in Eq. (2):

$$2H_2 \rightarrow 4H^{+} + 4e^{-} \quad (2)$$

O_2 undergoes a reduction reaction after it receives electrons at the cathode via Eq. (3):

$$O_2 + 4e^{-} \rightarrow 2O^{2-} \quad (3)$$

To complete the reaction, water should be formed by the following:

$$4H^{+} + 2O^{2-} \rightarrow 2H_2O \quad (4)$$

In the three different types of SOFC, due to the different conduction mechanisms of the electrolyte, the location of the generated water is different. H_2O is generated on the anode in O–SOFC, but on the cathode in P–SOFC. In the case of D-SOFC, H_2O is formed on both anode and cathode.

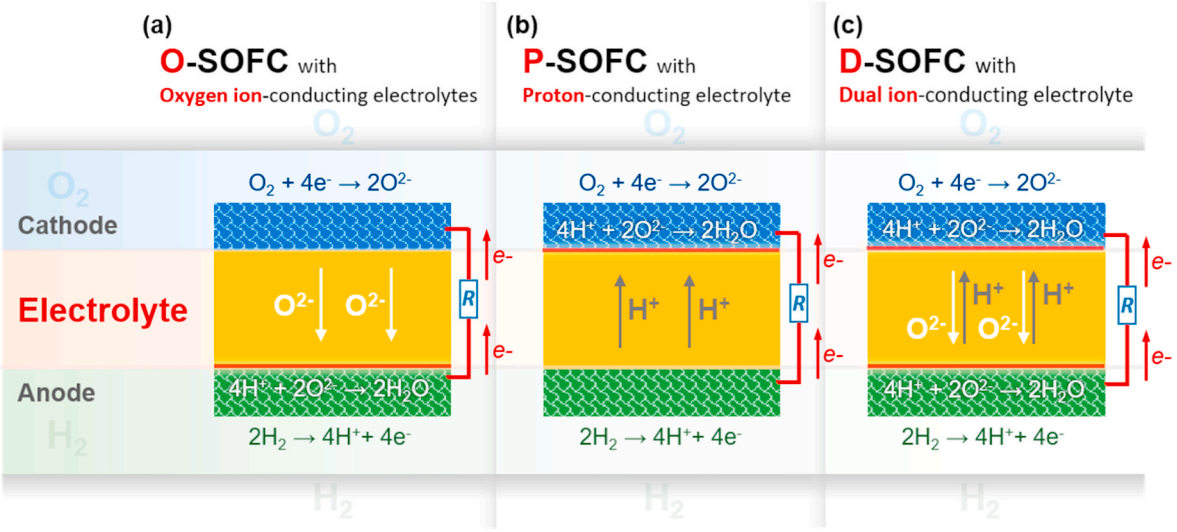

Fig. 1. Schematic diagrams of the working principles for (a) O–SOFC, (b) P–SOFC and (c) D-SOFC.

2.1. Oxygen ion-conducting electrolytes

In O–SOFCs, the electrolyte layer transports oxygen ions from the cathode to the anode. In order to reach favorable power output, the electrolyte materials should have high ionic conductivity at their working temperature range. Moreover, since the electrolyte layer is interposed between the anode and the cathode, facing the oxidizing and reducing atmospheres respectively, the electrolyte material is required to be densely sintered and have good mechanical and chemical stability. The conduction of oxygen ions in a dense solid material normally depends on the lattice defects and is driven by a concentration gradient or current.

2.1.1. Stabilized ZrO_2

At present, the most widely used oxygen ion-conducting electrolyte materials for IT-SOFCs are fluorite-type oxides, which possess a face centered cubic arrangement of cations with anions occupying all the tetrahedral sites. When a small number of lower valence cations are introduced into the crystal structure, the crystal will maintain the fluorite structure and generate some oxygen ion vacancies, which provide a channel for the conduction of oxygen ions. The fluorite-structured materials that can be used as an electrolyte for IT-SOFCs are predominantly stabilized ZrO_2, doped CeO_2, and stabilized Bi_2O_3.

Pure ZrO_2 exhibits three different crystal structures, i.e. monoclinic (<1170 °C), tetragonal (1170–2370 °C) and cubic (>2370 °C) [16]. In the process of crystal structure transformation there is an accompanying change in the crystal volume, which makes the thermal stability of pure ZrO_2 material very poor. The partial substitution of Zr by a suitable trivalent or divalent cation results in two beneficial effects: the creation of oxygen ion conductivity within the oxide lattice due to the introduction of oxygen vacancies, and stabilization of the cubic structure over a large temperature range, greatly improving the mechanical properties and thermal stability. As shown in Fig. 2, to compensate for the charge changes caused by the introduction of trivalent or divalent cations, oxygen vacancies are correspondingly generated in the crystal lattice, which provide a channel for oxygen ion conduction. Y is the most popular dopant for ZrO_2. At present, YSZ is the most widely used electrolyte in high-temperature SOFCs, especially for world-wide commercial SOFC stacks with a power range from 1 KW to 1 MW [17–19]. As a state-of-the-art electrolyte material for SOFCs, its properties have been well studied, including optimal doping amount, structural stability, and sintering performance. Based on the investigation of Badwal, it was found that the bulk conductivity was significantly dependent on the concentration of oxygen vacancies, which are determined by the doping amount. The results showed that, at lower concentration, as the doping level increased, the conductivity increased and reached a maximum at 8%; however, the oxygen ion conductivity greatly decreased if the doping amount was more than 8%, especially at lower temperatures [20].

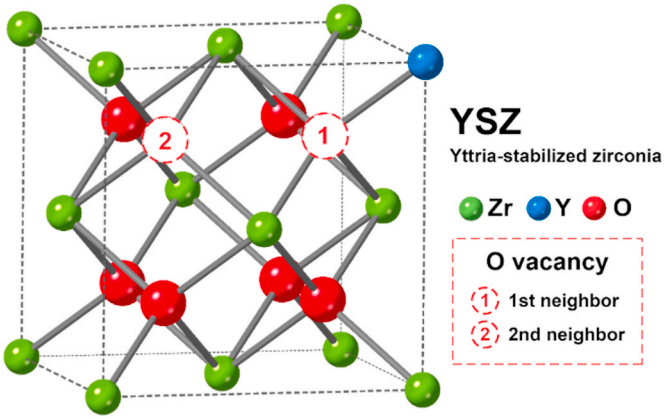

Fig. 2. Schematic of the defect fluorite structure in YSZ.

Even for the 8% Y-stabilized ZrO_2, the ionic conductivity decreases rapidly with decreasing temperature. As a result, when using YSZ material as the electrolyte for IT-SOFCs, the membrane must be thin enough to maintain low ohmic resistance [21]. In order to obtain favorable power output of the IT-SOFCs, the area-specific resistance (ASR) of the electrolyte layer should maintain a low value. Taking 0.2 Ω cm^2 as a target, the maximum thickness of the electrolyte layer can be calculated using the following formula:

$$L = 200 \times \sigma \quad (5)$$

where L (μm) is the electrolyte layer thickness, and σ is the ionic conductivity (S cm^{-1}) of the corresponding temperature. As shown in Fig. 3, the conductivity of YSZ at 500 °C is approximately 0.0005 S cm^{-1}, meaning that the thickness of the YSZ electrolyte layer should be less than 1 μm to reach the ohmic resistance of 0.2 Ω cm^2 [22]. To fabricate a dense YSZ thin film with such a small thickness, advanced technology must be adopted. For example, An et al. reported an SOFC with a thin-film YSZ of only 50 nm. The peak power density (PPD) of the cell reached as high as 1.3 W cm^{-2} at 450 °C, operating on H_2 fuel [23]. However, the mass production of electrolyte layers with a thickness less than 1 μm is a big challenge, especially for scaling up to large-size cells.

The results suggest that the ionic conductivity of stabilized zirconia should be further improved in order to realize its application in IT-SOFCs. Following this, different dopants were extensively trialed for zirconia oxides. Studies have shown that doping trivalent ions (rare earth metals) are more effective than divalent ions (alkali metals), mainly because of the higher defect association tendency and the lower thermodynamic stability of cubic fluorite [29,30]. For trivalent ions, the doping effect on oxygen ion conductivity is mainly in the order of Eu < Gd < Dy < Y < Er < Yb < Sc [31]. Among them, Sc_2O_3-stabilized ZrO_2 (ScSZ) demonstrated the highest ionic conductivity, reaching as great as 0.003 S cm^{-1} at 500 °C [24]. Together with the use of better electrodes, the SOFC with the thin-film ScSZ electrolyte has demonstrated a favorable power output at intermediate temperature [32–34]. Unfortunately, scandium-rich minerals are scarce. The separation and extraction of scandium is also very difficult, which makes scandium and its

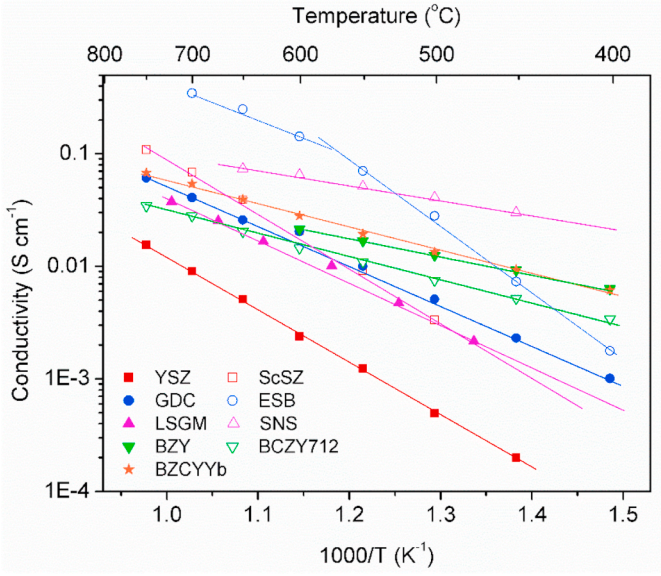

Fig. 3. Ionic conductivity versus reciprocal temperatures for selected electrolyte materials, including 8 mol% Y_2O_3–ZrO_2 (YSZ) [22], 8 mol% scandia stabilized ZrO_2 (ScSZ) [24], $Gd_{0.1}Ce_{0.9}O_{1.95}$ (GDC) [22], $Er_{0.4}Bi_{0.6}O_3$ (ESB) [25], $La_{0.8}Sr_{0.2}Ga_{0.8}Mg_{0.2}O_{3-\delta}$ (LSGM) [26], $Sr_{0.55}Na_{0.45}SiO_{2.755}$ (SNS) [27], $BaZr_{0.8}Y_{0.2}O_{3-\delta}$ (BZY) [28], Ba $Ce_{0.7}Zr_{0.1}Y_{0.2}O_{3-\delta}$ (BCZY712) [22] and $BaZr_{0.1}Ce_{0.7}Y_{0.1}Yb_{0.1}O_{3-\delta}$ (BZCYYb) [22].

compounds expensive and affects its large-scale application. Compared to Sc_2O_3, Er_2O_3 and Yb_2O_3 are much cheaper and the ionic conductivity of ZrO_2 stabilized with Er_2O_3 or Yb_2O_3 is still acceptable. Therefore, they (Sc- or Yb-stabilized zirconia) are more promising for reduced temperature SOFCs. However, one big challenge for IT-SOFCs with stabilized ZrO_2 electrolytes is the very limited choice of cathode materials. It was found that cathodes containing Ba, La and other elements react easily with YSZ, which causes a substantial increase in both electrode polarization resistance and ohmic resistance, as well as poor long-term stability of the cells [35,36]. A buffer layer may be applied to avoid direct contact between the YSZ electrolyte and the cathode. It should have high oxygen-ionic conductivity and chemical inertness towards both the electrolyte and the cathode. Currently, doped ceria is widely applied as the buffer layer [35–39].

2.1.2. Doped CeO_2

Different to the multiphase nature of ZrO_2, CeO_2 maintains its cubic fluorite structure from room temperature to its melting point. However, pure CeO_2 has negligible oxygen vacancies in its crystal structure, so the oxygen ion conductivity is very low. In order to improve its oxygen ion conductivity at intermediate temperatures, the partial substitution of Ce^{4+} in the crystal structure with a trivalent or divalent cation such as Gd^{3+}, Sm^{3+}, Y^{3+}, La^{3+} or Ca^{2+} has been investigated extensively, leading to the generation of more oxygen vacancies that are the carriers of oxygen ions. Studies have shown that the closer is the ion radius of the dopant cation to Ce^{4+}, the higher is the expected oxygen ion conductivity [40,41]. Kim proposed the concept of a critical ionic radius (r_c) for the dopant. For CeO_2 with trivalent dopants, the value of r_c is 1.038 Å [42]. Among these doped CeO_2 oxides, $Gd_{0.1}Ce_{0.9}O_{1.95}$ (GDC) and $Sm_{0.2}Ce_{0.8}O_{1.9}$ (SDC) have the highest ionic conductivity and are used in IT-SOFCs.

Doped CeO_2 materials have much higher oxygen ion conductivity than stabilized ZrO_2, especially at intermediate temperatures. It is worth noting, in the literature, that there are many studies of the conductivity of doped CeO_2 electrolytes, but the reported conductivity varied quite significantly. There are two main reasons for such a discrepancy. One is the relative densities of the electrolytes and the other is the impurities in the electrolytes. The sintering of the electrolyte layer is related to the properties of the initial powder and the sintering temperature. Adding Al_2O_3, ZnO, Fe_2O_3, etc. can effectively improve the sintering performance of doped CeO_2. Consequently, higher oxygen ion conductivity is achieved [43–46]. The purity of the electrolyte is another important issue. The common impurity in the electrolyte is silicon oxide, which is ubiquitous in chemicals, water and the environment. The studies found that silicon oxide usually deposits at the grain boundaries of the sintered electrolyte, which hinders the conduction of oxygen ions at the grain boundaries [47,48]. Therefore, during electrolyte preparation, the purity of the product, the silicon content of the liquid used, and the sintering environment should be strictly controlled. In order to obtain better electrolyte performance, co-doping methods are sometimes used and materials such as $Ce_{0.8}Pr_{0.2-x}La_xO_{2-\delta}$, $Ce_{1-x-y}Dy_xCa_yO_{2-\delta}$, and $Ce_{1-x}(Sm/Gd)_xO_{2-\delta}$ have shown favorable conductivity at intermediate temperatures. Through systematic optimization, the sintering performance and conductivity of the doped CeO_2 electrolyte have been improved [49–51].

In addition to higher oxygen ion conductivity, doped CeO_2 electrolytes show good chemical compatibility with many cathodes, like $La_{0.6}Sr_{0.4}Co_{0.2}Fe_{0.8}O_{3-\delta}$ (LSCF), $Ba_{0.5}Sr_{0.5}Co_{0.8}Fe_{0.2}O_{3-\delta}$ (BSCF), $Sm_{0.5}Sr_{0.5}CoO_{3-\delta}$ (SSC) and others, in the low to intermediate temperature range. Many IT-SOFCs with a thin-film-doped CeO_2 electrolyte have demonstrated low overall cell resistance and have delivered favorable PPD at temperatures down to 500 °C [52–55]. In particular, the ionic conductivity of GDC can reach as high as 0.005 S cm^{-1} at 500 °C, which is one order of magnitude that of YSZ at the same temperature [22]. It suggests that the thickness of the electrolyte layer must be no more than 10 μm in order to reach an ASR of 0.2 Ω cm^2 for the ohmic resistance. A thin film with such thickness can be easily fabricated on a large scale using a low cost process like tape casting, screen printing, or spin coating. For example, Zhang et al. fabricated a cell with an anode-supported doped electrolyte (~12 μm) and BSCF cathode based on screen printing of the electrolyte layer, which delivered a high PPD of 370 mW cm^{-2}, with H_2 as fuel, at 505 °C [56].

One big concern in the use of a doped ceria electrolyte is partial electronic conductivity at elevated temperature and reduced atmosphere, which is related to the reduction of Ce^{4+} to Ce^{3+}. Such partial electronic conductivity causes a decrease in the open circuit voltage (OCV) and reduces overall Faradaic efficiency of the IT-SOFCs. In particular, for a thin-film electrolyte, such internal shorted current becomes more obvious. For example, Zhang et al. analyzed the internal shorting of a thin-film SDC electrolyte cell [57]. At 600 °C, the respective OCV values were 0.84 V, 0.87 V, and 0.91 V for a cell with an electrolyte thickness of 10 μm, 20 μm, and 400 μm. Thus, it is generally considered that the doped ceria thin-film electrolyte is suited for operation at a temperature of 600 °C or lower. Therefore, IT-SOFCs based on a doped ceria thin-film electrolyte are usually operated at the temperature range of 450–600 °C. One way to broaden the application temperature range of a doped ceria electrolyte is the use of an electron block layer [58–60]. As shown in Fig. 4, Su et al. fabricated an SOFC with the SDC electrolyte and a proton-conducting oxide as the ionic conducting phase in the anode. An *in situ* phase reaction occurred between the SDC and the proton-conducting oxide to form a thin buffer layer that suppressed the internal shorting of the SDC. Therefore, the OCV of the SOFCs with an SDC electrolyte was successfully increased to 1.02 V at 600 °C while excellent power outputs were maintained (a PPD of 574 mW cm^{-2} at 600 °C) [58].

2.1.3. Bi_2O_3-based electrolytes

To further reduce the operation temperature of SOFCs to lower than 450 °C, doped ceria oxides are not suitable as electrolytes because of the insufficiency of their ionic conductivity under such conditions. Bi_2O_3-based oxides then became a focus of attention due to their superior conductivity. The pristine Bi_2O_3 has three different crystal structures, i.e. monoclinic (α-Bi_2O_3), tetragonal (β-Bi_2O_3) and cubic (δ-Bi_2O_3). Among these structures, δ-Bi_2O_3 is stable from 730 to 804 °C, and possesses a defective fluorite structure in which two of the tetrahedral sites are unoccupied [61]. Some dopants, like Y^{3+}, Pr^{3+} and Er^{3+}, can stabilize the cubic structure of δ-Bi_2O_3 at room temperature. Therefore, some stabilized δ-Bi_2O_3 oxides have shown higher oxygen ion conductivity than doped ceria, as well as excellent oxygen surface exchange kinetics that can promote oxygen migration/diffusion at the cathode-electrolyte interface [62–65]. However, to date, stabilized δ-Bi_2O_3 has seldom been applied as the electrolyte in IT-SOFCs due to the fact that bismuth oxide has relatively poor chemical stability. It is easily reduced to Bi metal under a reducing atmosphere. In addition, due to the low melting point and easy volatilization of Bi_2O_3 at high temperatures, the stabilized Bi_2O_3 electrolyte rarely becomes densified and it usually has poor mechanical strength [66,67]. Other bismuth oxide-based electrolyte materials, like the γ-$Bi_4V_2O_{11}$ series oxides, also show favorable oxygen-ion conductivity at reduced temperatures. After the partial replacements of V by Cu, Ni, Zn, Fe and Co, the oxides maintain their tetragonal crystal structure, while their conductivity is improved at reduced temperatures. However, such materials are susceptible to reaction with other materials, and their high thermal expansion coefficients (TECs) and poor mechanical properties are also big concerns for practical use in IT-SOFCs [68–70]. Considering the poor chemical stability of Bi_2O_3-based oxides under a reducing atmosphere, the concept of a dual-layer electrolyte was proposed, which takes advantage of the superior oxygen ion conductivity of Bi_2O_3 oxides and solves the problem of insufficient stability under a reducing atmosphere [25,71–73].

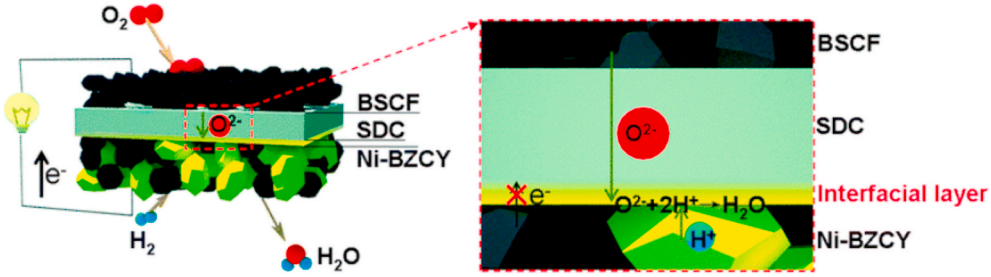

Fig. 4. Schematic of the SOFC with beneficial anode-electrolyte interfacial reaction. Reproduced with permission from Ref. [58]. Copyright 2012, Royal Society of Chemistry.

2.1.4. *$LaGaO_3$-based perovskite-type electrolytes*

ABO_3-type perovskites are a large category of oxides in which A is a lanthanum or alkaline earth element and B is a transition metal element. Many perovskite oxides show mixed oxygen ion and electronic conductivity and they have been extensively used as electrode materials in SOFCs, especially as cathode materials. Some perovskite-type or related materials, like $LnBO_3$ (B = Al, In, Sc, Y) perovskites, doped $LaGaO_3$ perovskites, $La_2Mo_2O_9$ and brownmillerite-like phases (with the chemical formula of $A_2B_2O_5$), have shown high and pure oxygen ion conductivity at intermediate temperatures, making them suitable for use as electrolyte materials for IT-SOFCs. Among these oxides, $LaGaO_3$-based perovskite oxides were most intensely investigated as electrolytes for IT-SOFCs [26,74–76]. If the A site of $LaGaO_3$ is doped with divalent alkaline earth metal ions, like Sr^{2+}, Ba^{2+}, and Ca^{2+}, oxygen vacancies will be generated. Research shows that the partial substitution of La^{3+} with Sr^{2+}, which has the closet ionic radius to La^{3+}, results in the highest oxygen ion conductivity. Theoretically, as the amount of A-site doping increases, the number of oxygen vacancies should increase and thus the oxygen ion conductivity increases. However, in practice, the amount of Sr^{2+} doping in the A site is limited. For example, if the doping amount of Sr^{2+} is higher than 10%, in addition to the main perovskite phase, $SrGaO_3$ or La_4SrO_7 impurity phases are also found, which negatively affects the oxygen ion conduction. Doping the B site of $LaGaO_3$ with divalent ions will also encourage oxygen vacancies. After doping Mg^{2+} into the B site, additional oxygen vacancies will be created, and the ionic conductivity improves rapidly. Meanwhile, the doping of Ga^{3+} with Mg^{2+} also increases the doping limit of La^{2+} at the A site, which may be caused by the larger crystal lattice [77]. Ishihara et al. found that $La_{0.8}Sr_{0.2}Ga_{0.8}Mg_{0.2}O_{3-\delta}$ (LSGM) has the best oxygen ion conductivity among the $La_{1-x}Sr_xGa_{1-y}Mg_yO_{3-\delta}$ (x = 0.10–0.20, y = 0.15–0.20) series oxide electrolytes. It has higher oxygen ion conductivity than stabilized ZrO_2 and is comparable to doped CeO_2 at intermediate temperatures [75]. Pelosato et al. prepared LSGM via a co-precipitation route in aqueous medium, and the sintered sample had a relative density of 98% and a total conductivity of 1.13×10^{-2} S cm^{-1} at 600 °C [26].

In spite of its high conductivity, the LSGM electrolyte has been used less in IT-SOFCs than doped ceria. This is due to several challenges for IT-SOFCs based on an LSGM electrolyte. Firstly, LSGM is very difficult to densify. Secondly, very often, an impurity phase could be formed during the synthesis of LSGM perovskite, which inevitably reduces the apparent conductivity. Thirdly, LSGM easily reacts with Ni-based cermet and forms a low conductivity phase at the interface [78]. To avoid a reaction between the anode and the LSGM electrolyte, a perovskite oxide or a low temperature-sintered Ni-based anode is a good choice [79–81]. For example, Huang et al. have developed a double-perovskite anode, $Sr_2MgMoO_{6-\delta}$, based on the LSGM electrolyte. With hydrogen or methane as its fuel, the single cell has high power density and a stable performance on power cycling [80].

2.1.5. *Other oxide electrolytes*

In addition to the above-mentioned oxide electrolytes, a series of oxide compounds with a 2D layered structure, firstly reported by Goodenough et el., also show favorable oxygen ion conductivity at intermediate temperatures, which can be used as electrolytes for IT-SOFCs [27,82–92]. These oxides have the structural formula of $Sr_{1-x}A_xSi_{1-y}Ge_yO_{3-0.5(x+y)}$ (A = Na or K). Research has shown that K-doped samples in this system were subsequently highly hygroscopic at room temperature, while Na-doping, with the large range of solubility of Na ions on the Sr site, proved to be highly effective in introducing pure oxygen ion conduction into the system [83]. The best oxide ion conductivity of the $Sr_{1-x}A_xSi_{1-y}Ge_yO_{3-0.5(x+y)}$ (A = Na or K) series was found in the composition $Sr_{0.55}Na_{0.45}SiO_{2.755}$ (SNS). At 500 °C, the measured oxide ion conductivity reached $>10^{-2}$ S cm^{-1} [27]. It is worth noting that the oxygen ion conduction activation energy of SNS is only 0.3 eV, which is much lower than that of traditional oxygen ion conductors based on oxygen vacancies. As shown in Fig. 5a, no apparent p_{O2}-dependence of conductivity was observed over a p_{O2} window as wide as 10^{-30} to 1 atm, suggesting that SNS is indeed a pure and chemically stable oxide ion conductor. No obvious change in conductivity was observed with respect to oxidizing or reducing atmospheres for 200 h, as seen in Fig. 5b, indicating that the oxide ion-conducting phase in SNS is stable. With H_2 as fuel, an electrolyte-supported SOFC with an SNS layer of 294 mm and infiltrated electrode nanoparticles (anode: Ni + SNS, cathode: $Sm_{0.5}Sr_{0.5}CoO_{3-\delta}$ + SNS) has an OCV of above 1.10 V and PPD of 213 mW cm^{-2} at 500 °C. Due to its high conductivity, the SNS electrolyte has a greater advantage at lower temperatures. If the fuel cell structure could be optimized in anode–supported form, even better performance could be achieved. However, at present, there are still problems in the selection and matching of anodes and cathodes with SNS electrolytes, and the stability of SNS materials during thermal cycling is poor. These are the aspects that need to be improved in future studies.

2.2. *Proton-conducting electrolyte*

Normally, the conductivity of oxygen ion-conducting electrolytes sharply reduces with a decrease in operation temperature, due to the high activation energy (E_a) of oxygen ion conductors. Whereas proton conductors, as the name suggests, possess proton conductivity with an appropriate conductivity value in the intermediate to low temperature ranges under an atmosphere containing vapor (~0.01 S cm^{-1} at 600 °C) [93]. There are mainly two proton transport mechanism for proton-conducting electrolyte, the vehicle mechanism and the Grotthuss mechanism [94]. In the vehicle mechanism, a proton attaches itself to an oxygen ion to form hydroxide ion (OH^-), which moves instead of the individual proton. This proton transport mechanism is attributed to the movement of OH^- by oxygen vacancies. The Grotthuss mechanism is essentially a two-step mechanism which involves the reorientation of the OH^- and proton transfer between adjacent oxygen ions. Unlike vehicle mechanism, in Grotthuss mechanism, the proton is the only mobile species while the oxygen is localized in the vicinity of its crystallographic position. Generally, they have a much lower E_a (0.4–0.6 eV) than that of oxygen ion conductors [95,96]. Therefore, compared with oxygen ion-conducting oxides, the proton-conducting materials are more suitable as the electrolytes of intermediate to low temperature

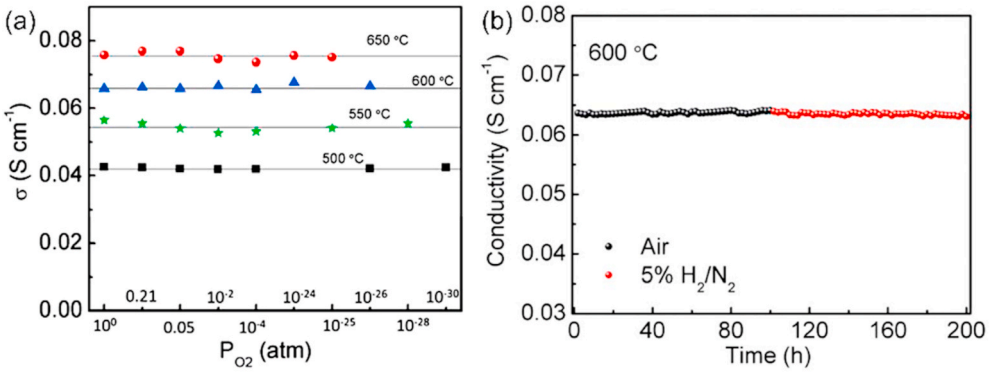

Fig. 5. (a) Variation of oxide ion conductivity of SNS with p_{O2} at 500–650 °C, and (b) stability of SNS in air and dry 5% H_2–N_2. Reproduced with permission from Ref. [27]. Copyright 2014, Royal Society of Chemistry.

SOFCs (ILT-SOFCs), which has led to an important development trend for SOFCs.

In the early 1980s, for the first time, Takahashi and Iwahara found that $SrZrO_3$-based materials possessed high temperature proton conductivity [97]. Immediately after, Iwahara et al. reported that doped $SrCeO_3$ exhibited proton conductivity when it was exposed to a water- or hydrogen-containing atmosphere [98,99]. However, $SrCeO_3$-based materials usually show low ionic conductivity and their chemical stability is also weak, leading to decomposition to $SrCO_3$ and CeO_2 under CO_2 atmosphere at high temperatures. Later, they systematically investigated the high temperature proton-conducting properties of acceptor-doped $BaCeO_3$ [100–103]. Since then, the researchers began to pay attention to this kind of electrolyte material that can conduct protons. Up to now, many protonic ceramics with various structures have been developed, including ABO_3 simple perovskite, and $A_2B_2O_5$ brownmillerite, as well as $LnBO_4$ orthophosphates, orthoniobates and orthotantalates [104, 105]. The ABO_3 simple perovskite is the most popular proton-conducting electrolyte material among these structures, because its crystal structure is beneficial for proton mobility, thus a high ionic conductivity can be expected. Doped $BaCeO_3$ and $BaZrO_3$ are two types of representative and promising proton-conducting electrolyte. By substituting the B-site ions of $BaCeO_3$ and $BaZrO_3$ with dopants such as Y ion, oxygen vacancies are formed, which are the sites for hydrogen incorporation and transportation. Hence, the protonic defects are created through dissociative adsorption of the water.

2.2.1. *Doped $BaCeO_3$*

We know that an excellent electrolyte material should meet three requirements: high ionic conductivity, strong chemical stability and good sinterability. The proton conductivity of $BaCeO_3$-based electrolytes is generally high, with values of greater than 0.01 S cm^{-1} among inorganic proton conductors. Furthermore, doped $BaCeO_3$ shows satisfactory sinterability [93]. Therefore, doped $BaCeO_3$ materials are currently one of the most widely studied proton conductors. All the rare earth elements have been partially doped in the B-site of $BaCeO_3$, and their physico-chemical properties, such as crystal structure, electronic conductivity, and chemical stability have been investigated in detail [106–110]. Medvedev et al. have reviewed the development, properties and application of $BaCeO_3$-based materials [111]. Similar to doped $SrCeO_3$ materials, their poor chemical stability hinders the practical application of $BaCeO_3$-based materials. Due to the natural basicity of barium cerate, they easily react with acidic gases (CO_2 and SO_2) and H_2O to produce $BaCO_3$, $BaSO_4$ and $Ba(OH)_2$, which can hamper the proton migration, resulting in large thermal expansion of the materials, thus greatly reducing the performance of fuel cells.

Matsumoto et al. investigated the effects of different dopants including Y^{3+}, Yb^{3+}, Tm^{3+}, Lu^{3+}, In^{3+}, and Sc^{3+} on the conductivity and stability of $BaCeO_3$ [112]. It was found that, with the increase of ionic radius of dopants, the ionic conductivity was enhanced but the chemical stability decreased. In other words, the Y^{3+}-doped $BaCeO_3$ (BCY) showed the best conductivity, while Sc^{3+}-doped $BaCeO_3$ demonstrated a better stability among all the studied oxides. Although BCY possesses high proton conductivity, the SOFCs with a majority of the proton-conducting electrolytes still showed lower cell performance as compared with oxygen ion-conducting SOFCs at low temperatures, which is mainly attributable to the lack of matched cathode materials and the relatively low conductivity produced. As shown in Fig. 6, Liu et al. improved the performance of BCY via a Pd ingress-egress approach to design a new proton-conducting perovskite with the composition of $BaCe_{0.8}Y_{0.1}Pd_{0.1}O_{3-\delta}$ (BCYP10). The introduction of a small amount of Pd resulted in a great increase in ionic conductivity, thus the SOFC with a BCYP10 electrolyte delivered a high PPD of 645 mW cm^{-2} at 700 °C [113]. As to the enhancement of chemical stability, it is hard to find a smaller trivalent rare earth cation than Sc^{3+}, so the chemical stability of $BaCeO_3$ cannot be further improved by doping with other rare earth cations. However, the expensive price of Sc prevents its widespread application. Therefore, Shin et al. recently investigated the effects of Al^{3+} doping into $BaCeO_3$ upon its chemical stability and conductivity properties [114]. They found that Al-doped $BaCeO_3$ delivered better chemical stability than that of rare earth metal cation-doped $BaCeO_3$. Although the protonic conductivity of Al-doped $BaCeO_3$, as a whole, is lower than that of BCY at 250–800 °C, its conductivity at 400–470 °C has exhibited an abnormal phenomenon that is comparable to that of BCY in that there is a transformation of crystal structure and a dehydration reaction occurs with the changes in temperature. Bi et al. co-doped Ta and Y into the Ce site of $BaCeO_3$ to form $BaCe_{0.7}Ta_{0.1}Y_{0.2}O_{3-\delta}$, which delivered an acceptable chemical stability against H_2O and CO_2 [115]. It indicated that a Ta-doping strategy is promising to balance the conductivity and chemical stability. It should be mentioned that some of the doped $BaCeO_3$ perovskites showed mixed oxygen ion and proton conductivities at elevated temperatures. This will be discussed in a later section.

2.2.2. *Doped $BaZrO_3$*

In contrast to $BaCeO_3$-based materials, doped $BaZrO_3$ is much more stable in acidic gases or a steam-containing atmosphere [116]. However, $BaZrO_3$-based electrolytes face a big challenge because of their inability to form a dense membrane. Due to the poor sinterability of $BaZrO_3$, after sintering, the samples usually show low density and high grain boundary resistance, leading to low total proton conductivity [27]. Fortunately, the drawbacks of $BaZrO_3$ can be overcome by introducing sintering aids, such as using ultrafine powder precursors, or adopting advanced thin-film fabrication techniques.

The Y ion has been considered as the best dopant for the B-site of $BaZrO_3$ until now. Kreuer et al. demonstrated that doping with Y did not change the hydration enthalpy and mobility of protonic defects, when

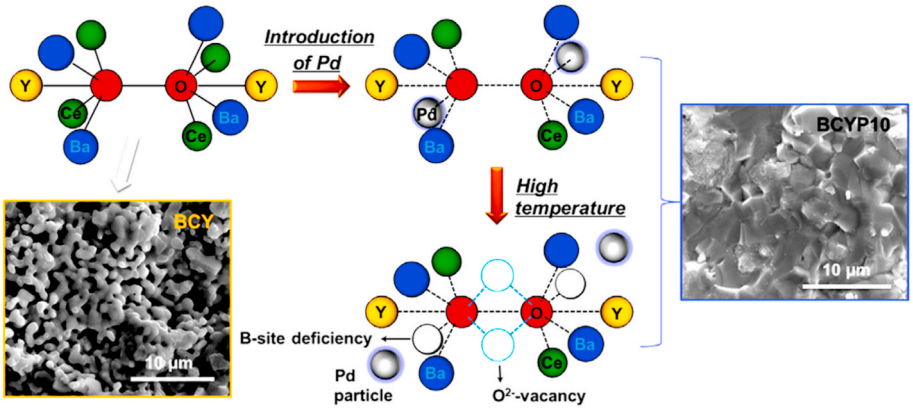

Fig. 6. Mechanism of the sintering process for a BCY electrolyte with Pd. Reproduced with permission from Refs. [113]. Copyright 2014, Elsevier.

compared with undoped $BaZrO_3$ [117]. Therefore, Y-doped $BaZrO_3$ (BZY) is one of the most popular barium-zirconate materials. It is almost a pure proton conductor in H_2 and/or vapor-containing atmospheres at low temperatures (such as less than 650 °C) [27]. The application of sintering aids is commonly used to enhance the sinterability of BZY [118–122]. Solid-state reactive sintering (SSRS) is an effective method to fabricate dense pellets [123]. The key point of SSRS is the introduction of sintering aids with raw precursors. Prof. O'Hayre's group at the Colorado School of Mines optimized the SSRS approach to fabricate P–SOFCs in one firing step with the help of a NiO sintering aid [124]. The dense BZY membrane, fabricated at a relatively low temperature of 1400 °C, showed a high total conductivity of 3.3×10^{-2} S cm^{-1} at 600 °C in a wet argon atmosphere [125]. The P–SOFC with BZY electrolyte yielded a PPD of 335 mW cm^{-2} at 500 °C, using H_2 fuel [124].

The preparation of an ultrathin BZY electrolyte layer using pulsed laser deposition (PLD) and atomic layer deposition (ALD) is beneficial to decrease the ohmic resistance of P–SOFCs, realizing a good cell performance [126,127]. Bae et al. fabricated a P–SOFC with a thin-film BZY electrolyte (~2 μm) using the PLD technique. No impeding grain boundaries were proven, thus the fuel cell showed a super high power output (PPD of 740 mW cm^{-2} at 600 °C) among the reported P–SOFCs with BZY electrolytes in the literature, as shown in Fig. 7 [128]. However, these techniques are not suitable for large-scale applications at present, and they will also increase the fabrication cost.

As mentioned earlier, the doping strategy involves oxygen vacancies in the lattice, then promotion of the protonic conductivity of oxides [129]. Sometimes, an improvement in sintering properties can be achieved due to the effect of a dopant [130]. Fabbri et al. developed a new proton conductor by partially substituting Zr ions with Pr ions, i.e. $BaZr_{0.7}Pr_{0.1}Y_{0.2}O_{3-\delta}$ (BZPY) [93]. It demonstrated both strong chemical stability and high proton conductivity (2×10^{-2} S cm^{-1} at 600 °C under wet air). Moreover, improved sinterability was revealed, compared with BZY. Although the P–SOFC with BZPY electrolyte achieved low performance, it could be increased by the development of matched cathode materials. Sun et al. doped 10 mol% Sn in the B-site of BZY to form $BaZr_{0.7}Sn_{0.1}Y_{0.2}O_{3-\delta}$ (BZSY) and demonstrated its good chemical stability and sufficient conductivity with the value of 1.6×10^{-3} S cm^{-1} at 600 °C in wet H_2 containing 3% H_2O. The cell with the configuration of (anode) Ni + BZSY | BZSY (12 μm thickness) | $Sm_{0.5}Sr_{0.5}CoO_{3-\delta}$ + SDC (cathode) delivered a PPD of 360 mW cm^{-2} at 700 °C [131]. Liu et al. developed a $BaZr_{0.7}Nd_{0.1}Y_{0.2}O_{3-\delta}$ (BZNY) proton conductor, and both sinterability and conductivity of BZY were improved [132].

2.2.3. $BaCe_xZr_{1-x}O_3$-based electrolytes

According to the above statements, $BaCeO_3$ has high ionic conductivity and poor chemical stability, while $BaZrO_3$ shows the opposite trend. Therefore, the combination of $BaCeO_3$ and $BaZrO_3$ could effectively integrate their strengths while avoiding their shortcomings.

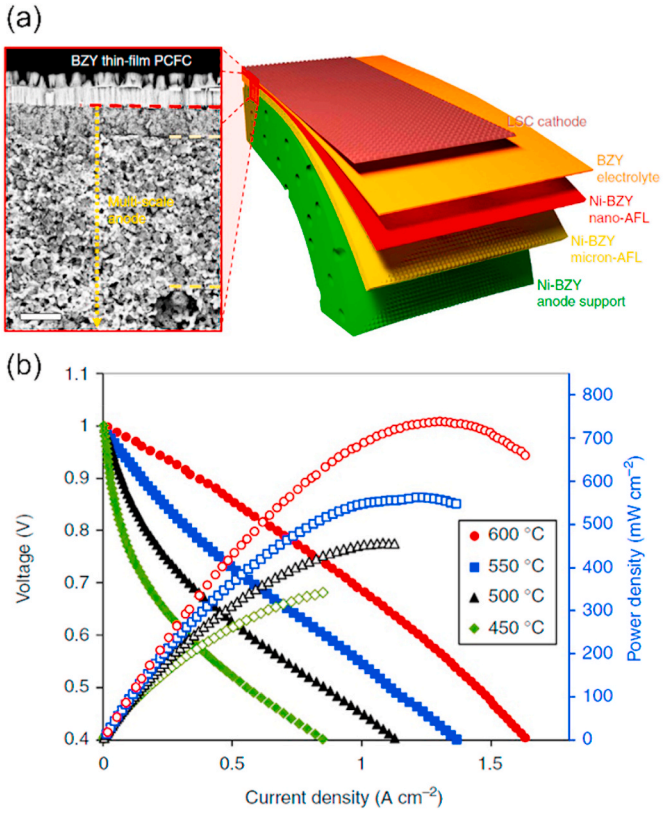

Fig. 7. (a) Structure configuration and (b) performance of the proposed P–SOFC with BZY thin layer. Reproduced with permission from Ref. [128]. Copyright 2017, Springer Nature.

Katahira et al. conducted a systematic study of Zr-doped BCY, i.e. $BaCe_{0.9-x}Zr_xY_{0.1}O_{3-\delta}$ (BCZY). As supposed, it was found that the increase in Ce content improved the conductivity and sinterability of BCZY, while the increase in Zr content enhanced the chemical stability of BZCY [116]. Consequently, $BaCe_{0.7}Zr_{0.1}Y_{0.2}O_{3-\delta}$ (BCZY712) became the most extensively used proton-conducting electrolyte, offering the best compromise between stability and conductivity [27,133]. However, later studies demonstrated that BCZY712 may not be very stable after long-term exposure to CO_2-containing atmosphere and boiling water [93,134]. It meant that further compositional optimization of BCZY was still necessary. Guo et al. carried out a systematic investigation concerning the effect of Zr doping on the performance of $BaZr_yCe_{0.8-y}Y_{0.2}O_{3-\delta}$ ($0.0 \leq y \leq 0.8$) for P–SOFCs [135]. They found that the anode-supported cell configuration was most favorable to thin-film

electrolyte sintering. After considering the sinterability, stability, and electrochemical activity of $BaZr_yCe_{0.8-y}Y_{0.2}O_{3-\delta}$, they believed that $BaZr_{0.4}Ce_{0.4}Y_{0.2}O_{3-\delta}$ (BZCY0.4) was a promising electrolyte material for P–SOFCs. Liu et al. further decreased the sintering temperature of BZCY0.4 dense pellets to 1250 °C via the infiltration of zinc nitrate solution as a sintering aid. The liquid phase mechanism is shown in Fig. 8. The total conductivity of BZCY0.4 + 4 wt% Zn was 0.40×10^{-2} S cm^{-1} at 600 °C in wet H_2 [136]. In addition to the BCZY series, the researchers also developed many other $BaCe_xZr_{1-x}O_3$-based electrolytes; for example, $BaCe_{0.9-x}Zr_xM_{0.1}O_{3-\delta}$ (M = Nd or Gd) [137], $BaCe_{0.4}Zr_{0.3}Sn_{0.1}Y_{0.2}O_{3-\delta}$ [138], $BaZr_{0.3}Ce_{0.5}Y_{0.2-x}Zn_xO_{3-\delta}$ [139], and so on. As a whole, although favorable conductivity could be achieved, the materials still suffered from the problems of poor sinterability, poor chemical stability and no matchable cathodes. More research studies are urgently needed for the development of IT-SOFCs based on proton-conducting electrolytes.

2.3. Dual ion-conducting electrolyte

The mixed conduction characteristics of the electrolyte and the co-existing electrochemical emissions in the anode and cathode make the D-SOFC a fascinating substitute for efficient energy conversion beyond the P–SOFC and O–SOFC. It is known that the harsh fuel dilution in O–SOFCs and the inevitable oxygen dilution in P–SOFCs, induced by the H_2O product, are severe challenges. By contrast, D-SOFCs enable a more harmonious electrochemical reaction between reducing and oxidizing gases, thanks to its dual ion conductivity in the electrolyte. Therefore, high cell performances could be triggered through the beneficial ionic transport process in the electrolyte, making D-SOFCs an impressive technological advancement in the future. There are currently two main types of dual ion-conducting electrolyte material: one is perovskite electrolytes and the other is ceria-carbonate composites. In both electrolyte materials, oxygen ions and proton conductivity exist at the same time, but the mechanism is different. We will discuss them separately below.

2.3.1. Perovskite electrolytes

As mentioned above, some doped $BaCeO_3$ proton-conducting materials have exhibited both the presence of oxygen ions and proton conductivity. In these perovskite lattices, the oxygen vacancies and proton defects act as the oxygen ion and proton carriers, separately. Actually, the oxygen ion conductivity could dominate over the proton conductivity under intermediate temperatures (600–800 °C) due to the hydrolysis effect. Additionally, these perovskite-type electrolytes are more likely to be the O^{2-} and H^+ co-conducting oxides within the intermediate temperature range. Iwahara et al. studied the doped $BaCeO_3$ electrolyte materials and found that some materials exhibit proton conductivity in a hydrogen atmosphere while becoming mixed ionic conductors of protons and oxide ions under fuel cell conditions (with hydrogen at the anode and oxygen at the cathode). By monitoring the water produced on the cathode and anode, with $BaCe_{0.9}Nd_{0.1}O_{3-\delta}$ as the electrolyte, the dual ion conduction of the electrolyte was confirmed [140]. As shown in Table 1, the transfer numbers of proton and oxygen ions were calculated based on the water evolution at each electrode. With the increase of operating temperatures, the amount of water produced on the cathode decreased, indicating that oxygen ion conduction dominates at high temperatures, while proton conduction dominates at lower temperatures. Peng et al. tested the conductivity of $BaCe_{0.8}Sm_{0.2}O_{2.9}$ (BCSO) and found that there was a clear turning point in the conductivity of the material at 550 °C under fuel cell conditions, due to the dual ion-conducting property [141]. Yang et al. proposed a famous dual ion-conducting electrolyte, $BaZr_{0.1}Ce_{0.7}Y_{0.1}Yb_{0.1}O_{3-\delta}$ (BZCYYb), which possessed excellent ionic mobility and good sinterability. As shown in the data in Fig. 3, conductivity as high as 0.013 S cm^{-1} was achieved at 500 °C [22]. Zhou et al. confirmed the dual ion-conducting property of the BZCYYb electrolyte for the first time [142]. With dry hydrogen as the fuel and flowing air as the oxidant, the absolute humidity was found to be 20.0 g m^{-3} in the anode chamber and 65.5 g m^{-3} in the cathode chamber. The cell performance was promoted

Table 1
Transference numbers of proton and oxide ions in $BaCe_{0.9}Nd_{0.1}O_{3-\delta}$ under fuel cell operating conditions [140].

	Temperature (°C)			
	700	800	900	1000
Oxide ion	0.22	0.58	0.71	0.79
Proton	0.78	0.42	0.29	0.21

Fig. 8. Schematic diagram of the liquid phase mechanisms that underlie the higher sinterability stimulated by ZnO. Reproduced with permission from Refs. [136]. Copyright 2013, Elsevier.

by a triple-conducting (proton, oxygen ion and electronic conduction) cathode of $Sr_2Sc_{0.1}Nb_{0.1}Co_{1.5}Fe_{0.3}O_{6-\delta}$ (SSNCF) and a PPD of 405 mW cm^{-2} was achieved at 500 °C.

2.3.2. *Doped CeO_2-carbonate composites*

Doped CeO_2 materials are oxygen ion-conducting electrolytes for SOFCs and molten carbonates are electrolytes for molten carbonate fuel cells (MCFCs). Zhu et al. found that the mixture of doped CeO_2 and carbonates (Li_2CO_3, Na_2CO_3, and K_2CO_3 or a mixture of these) with high dual ion conduction can be used as electrolytes for ILT-SOFCs [143–147]. The dual ion conduction of the doped CeO_2-carbonate composites was confirmed by performing DC-conducting measurements in different atmospheres. An example is SDC/Na_2CO_3. As shown in Fig. 9a, the nanocomposite electrolyte shows proton conductivity and oxygen ion conductivity within a temperature range of 200–600 °C. The DC conductivity of the SDC/Na_2CO_3 nanocomposite electrolyte reaches 0.02 S cm^{-1} in 5% H_2 and 0.002 S cm^{-1} in air at 500 °C. In this electrolyte, oxygen ions can transfer in the phase of SDC and protons are thought to be conducted between the carbonate and SDC phases. The pathway for proton conduction is shown in Fig. 9b, and the swing model of "Ce–O–H–O–C″ was believed to provide the possibility for proton conduction [144]. With H_2 as the fuel and air as the oxidant, a PPD as high as 750 mW cm^{-2} at 500 °C was achieved in a cell with an SDC-Na_2CO_3 composite electrolyte [145].

Because these electrolytes contain carbonates, the sintering temperature of these electrolytes must be strictly controlled. The presence of carbonate also promotes the sintering of the electrolyte and higher temperature will cause a loss of carbonate. The sintering temperature of single cells using this electrolyte is generally lower than 650 °C, and the operating temperature of the fuel cell should be lower than this temperature [148]. The carbonate vaporization and decomposition may result in performance degradation of SOFCs over long-term operation [149].

3. Conclusion, challenges and perspectives

A decrease in the operating temperature of SOFCs to the intermediate-to-low temperature range is vital for the widespread application of this attractive technology. A breakthrough in electrolyte materials is one of the key steps towards achieving this goal. An electrolyte material for IT-SOFCs should possess both high ionic conductivity at intermediate temperatures and good long-term stability under fuel cell operating conditions. Up to now, many oxide-based electrolyte materials have been developed or exploited as potential electrolytes for IT-SOFCs. These oxides are usually polycrystalline and form defined lattice structures, such as fluorite and perovskite. Oxygen vacancies are the main charge carriers of oxygen ions, while the proton conductivity is also closely related to oxygen vacancies. Introducing oxygen vacancies into the oxide lattice is a universal way to progress the development of oxide electrolytes for IT-SOFCs. The fluorite structure has been the most investigated structure for oxygen ion conductors, while stabilized zirconia and doped ceria have been the two most important examples of fluorite-type electrolytes. Dopants have been extensively applied to tailor the conductivity, stability, and sintering of the electrolyte materials. For zirconia-based materials, the dopant is also important to stabilize the cubic lattice structure. Different dopants usually have different effects on the properties and, thus, performance of the electrolytes. Typically, the more similar is the ionic radius of the dopant to the parent cation in the oxide, the higher is the conductivity that can be achieved. Perovskite-based oxides, like LSGM, are also an important type of oxygen ion electrolyte for IT-SOFCs. During the past, considerable research efforts have been directed towards this type of material. As compared to stabilized zirconia, LSGM shows higher ionic conductivity at intermediate temperatures, and it shows higher ion transfer numbers than doped ceria; thus it is highly attractive as an electrolyte in IT-SOFCs.

Compared to O–SOFC, P–SOFC is, in principle, more promising for reduced temperature applications since proton transfer requires lower activation energy than oxygen ion diffusion. Actually, P–SOFCs have received considerable attention recently and have become a hot research topic in the field of SOFCs. To date, the main proton-conducting electrolytes that have been developed are based on doped $BaZrO_3$ and $BaCeO_3$ parent perovskite oxides. After optimization, the conductivity of proton conductors is comparable to that of the benchmark oxygen ion-conducting electrolytes, like doped ceria and LSGM. The proton conduction in perovskite is also closely related to the oxygen vacancies. Under certain conditions, mixed oxygen ion and proton conduction could be created inside these perovskite oxides, leading to the development of a new type of dual ion-conducting SOFC, which also has received increasing attention recently.

Based on the previous works, we can see that all three kinds of available electrolyte material suffer from certain deficiencies, which could be derived from the intrinsic properties of the materials or a result of the preparation process. For example, the stabilized ZrO_2 electrolyte with high physico-chemical stability but low conductivity at low to intermediate temperatures limits its practical application in IT-SOFCs, while Bi_2O_3-based electrolyte materials, with extremely high ionic conductivity, are difficult to utilize in IT-SOFCs due to their poor stability. Doped CeO_2 is suitable for 450–600 °C but the internal current

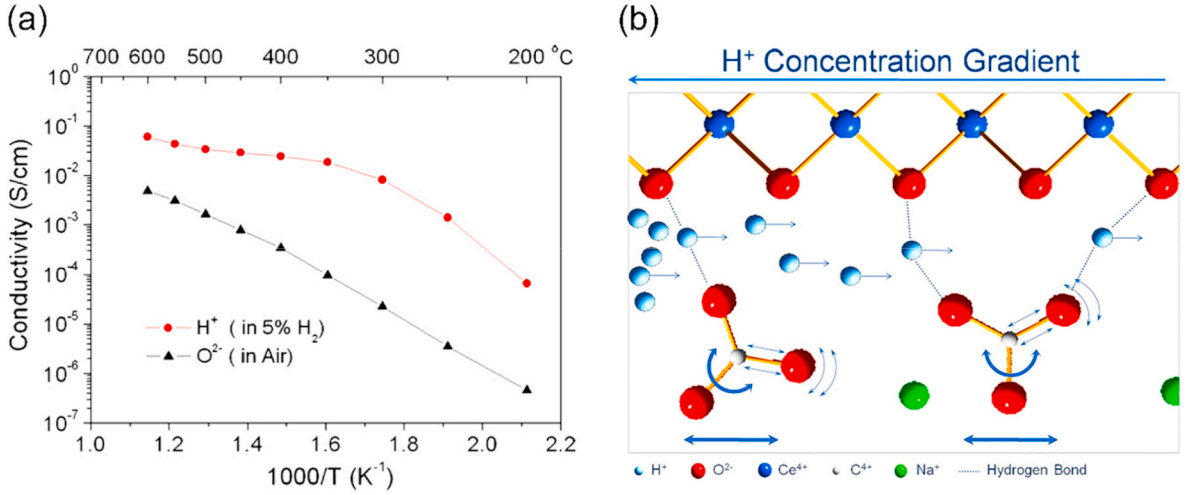

Fig. 9. (a) DC conductivity of SDC/Na_2CO_3 composite in 5% H_2 or air and (b) schematic of transfer of protons in the SDC/Na_2CO_3 composite. Reproduced with permission from Ref. [144]. Copyright 2011, Elsevier.

limits its application at temperatures higher than 600 °C, in particular in thin-film configuration. The LSGM and other perovskite electrolytes have also been questioned due to their stability issues. In contrast, the electrolyte materials with proton-conducting or dual-conducting abilities have low activation energy and can be used at intermediate to low temperatures (400–800 °C). By improving their physical and chemical stability, they are expected to become the first choice for low temperature SOFC electrolyte materials.

When compared to oxygen ion conductors, the easier migration of protons results in lower values of activation energy for proton conductors. Therefore, much attention has been paid to the SOFCs with a proton-conducting electrolyte because they are more suitable for operation at reduced temperatures. The main structure of proton-conducting electrolytes is perovskite oxide, such as $BaCeO_3$-based and $BaZrO_3$-based electrolytes. Despite the proton conductors showing a strong superiority, their big disadvantage is a lack of excellent materials concurrently possessing high proton conductivity and good chemical stability in an atmosphere containing CO_2, SO_2, and/or H_2O under SOFC operating conditions. In general, $BaCeO_3$-based electrolytes show high proton conductivity but poor chemical stability, while $BaZrO_3$-based electrolytes are exactly the opposite in delivering relatively low proton conductivity but strong chemical stability. The combination of $BaCeO_3$-based and $BaZrO_3$-based oxides to form new $BaCe_xZr_{1-x}O_3$-based electrolytes is a good option for the development of proton conductors. Currently, BCZY712 is a widely used and studied composition among many $BaCe_xZr_{1-x}O_3$-based electrolytes. Some $BaCeO_3$-based electrolytes (such as $BaCe_{0.9}Nd_{0.1}O_{3-\delta}$) also show oxygen ion conductivity alongside proton conductivity under certain circumstances, so they are actually dual ion electrolytes. The best known dual ion electrolyte is the perovskite BZCYYb. The other kind of dual ion electrolyte is a mixture of doped CeO_2 and carbonate composites, such as SDC/Na_2CO_3. Fuel cells with such an electrolyte have delivered attractive power output at low temperature. The dual ion electrolytes can combine the advantages of proton and oxygen ion conduction. Due to the dual ion conductivity, D-SOFCs no longer require an external humidification device, which can simplify the systems. By optimizing electrode materials and stability, D-SOFCs can achieve better performance at intermediate to low temperatures.

Considering the differences of these electrolytes in oxygen ion conductivity, chemical stability, and mechanical properties, sometimes their combined use can deliver better performances. For example, a thin layer of doped CeO_2 on stabilized ZrO_2 can avoid the potential reaction between the stabilized ZrO_2-based electrolyte and many high-performance cathode materials (such as BSCF and LSCF). This structure is being widely used at present, particularly as the main structure of the single cells in some running SOFC stacks. The LSGM layer on doped CeO_2 electrolyte can not only obtain a high open circuit voltage, but also avoid the interface reaction between the electrode and LSGM. The combination of stabilized ZrO_2 and δ-Bi_2O_3 can ensure the chemical and mechanical properties of the electrolyte and avoid the interface reaction, thus promoting the ORR performance at the cathode-electrolyte interface. The doped CeO_2 layer between anode and stabilized δ-Bi_2O_3 can block the electronic conductivity and avoid the reduction of stabilized δ-Bi_2O_3 at the anode-electrolyte interface. Sometimes, the structure of the electrolyte can be more complicated. A triple layer electrolyte may be designed to improve the performance of the IT-SOFC. Each layer of the electrolyte plays a separate role. Therefore, to enhance the performance and stability of SOFCs via the development and selection of electrolyte materials, the combined use of various electrolyte materials is a good choice.

On the other hand, the preparation technique is also very important for the fabrication of the electrolyte layer. Advanced manufacturing techniques, like pulse laser deposition, can reduce the thickness of the dense electrolyte layer, thereby improving the performance of SOFCs. Meanwhile, the cost of manufacturing technology is also important for large-scale applications and the quality of single cells should be controlled. With a decrease in operating temperatures, the problem of an increase in the ASR of electrodes will become more prominent. The development of adapted electrode materials must also be carried out synchronously. With the progress of these technologies, IT-SOFCs running at lower temperatures can be expected to yield commercial applications in the near future.

Declaration of competing interest

The authors declare that they have no known competing financial interests or personal relationships that could have appeared to influence the work reported in this paper.

Acknowledgements

This work was supported by Australian Research Council (ARC) Discovery Project Grants DP200103332 and DP200103315. Dr. Chao Su would like to thank the ARC Discovery Early Career Researcher Award DE180100773.

References

[1] H. Chen, T. Cong, W. Yang, C. Tan, Y. Li, Y. Ding, Prog. Nat. Sci. 19 (2009) 291–312.
[2] M. Kendall, Prog. Nat. Sci. 28 (2018) 113–120.
[3] W. An, X. Sun, Y. Jiao, S. Wang, W. Wang, M. Tadé, Z. Shao, S. Li, S. Shuang, Energy Fuels 32 (2018) 4559–4568.
[4] C. Su, W. Wang, R. Ran, Z. Shao, M. Tade, S. Liu, J. Mater. Chem. A 1 (2013) 5620–5627.
[5] H. Shi, Q. Li, W. Tan, H. Qiu, C. Su, Chin. J. Chem. Eng. 28 (2020) 1156–1161.
[6] A. Elleuch, K. Halouani, Y. Li, Fuel Cell 18 (2018) 206–218.
[7] A. Selimovic, M. Kemm, T. Torisson, M. Assadi, J. Power Sources 145 (2005) 463–469.
[8] T. Tsai, S. Barnett, Solid State Ionics 93 (1997) 207–217.
[9] W. Zhou, H. Shi, R. Ran, R. Cai, Z. Shao, W. Jin, J. Power Sources 184 (2008) 229–237.
[10] X. Kuai, G. Yang, Y. Chen, H. Sun, J. Dai, Y. Song, R. Ran, W. Wang, W. Zhou, Z. Shao, Adv. Energy Mater 9 (2019) 1902384.
[11] Y. Tian, Y. Liu, W. Wang, L. Jia, J. Pu, B. Chi, J. Li, J. Energy Chem 43 (2020) 108–115.
[12] S. Jiang, Int. J. Hydrogen Energy 44 (2019) 7448–7493.
[13] X. Xu, W. Wang, W. Zhou, Z. Shao, Small Methods 2 (2018) 1800071.
[14] P. Kaur, K. Singh, Ceram. Int. 46 (2020) 5521–5535.
[15] G. Yang, C. Su, H. Shi, Y. Zhu, Y. Song, W. Zhou, Z. Shao, Energy Fuels, in press, https://doi.org/10.1021/acs.energyfuels.0c01887.
[16] N. Mahato, A. Banerjee, A. Gupta, S. Omar, K. Balani, Prog. Mater. Sci. 72 (2015) 141–337.
[17] D. Yan, L. Liang, J. Yang, T. Zhang, J. Pu, B. Chi, J. Li, Energy 125 (2017) 663–670.
[18] L. Blum, L. Haart, J. Malzbender, N. Menzler, J. Remmel, R. Steinberger-Wilckens, J. Power Sources 241 (2013) 477–485.
[19] M. Yokoo, Y. Tabata, Y. Yoshida, H. Orui, K. Hayashi, Y. Nozaki, K. Nozawa, H. Arai, J. Power Sources 184 (2008) 84–89.
[20] S. Badwal, Solid State Ionics 52 (1992) 23–32.
[21] B. Steele, A. Heinzel, Nature 414 (2001) 345–352.
[22] L. Yang, S. Wang, K. Blinn, M. Liu, Z. Liu, Z. Cheng, M. Liu, Science 326 (2009) 126–129.
[23] J. An, Y. Kim, J. Park, T. Gür, F. Prinz, Nano Lett. 13 (2013) 4551–4555.
[24] D. Lee, I. Lee, Y. Jeon, R. Song, Solid State Ionics 176 (2005) 1021–1025.
[25] E. Wachsman, K. Lee, Science 334 (2011) 935–939.
[26] R. Pelosato, C. Cristiani, G. Dotelli, S. Latorrata, R. Ruffo, L. Zampori, J. Power Sources 195 (2010) 8116–8123.
[27] T. Wei, P. Singh, Y. Gong, J. Goodenough, Y. Huang, K. Huang, Energy Environ. Sci. 7 (2014) 1680–1684.
[28] E. Fabbri, L. Bi, D. Pergolesi, E. Traversa, Adv. Mater. 24 (2012) 195–208.
[29] A. Navrotsky, J. Mater. Chem. 15 (2005) 1883–1890.
[30] S. Ho, Mater. Sci. Eng. 54 (1982) 23–29.
[31] O. Yamamoto, Y. Arachi, H. Sakai, Y. Takeda, N. Imanishi, Y. Mizutani, M. Kawai, Y. Nakamura, Ionics 4 (1998) 403–408.
[32] H. Gu, R. Ran, W. Zhou, Z. Shao, J. Power Sources 172 (2007) 704–712.
[33] G. Cho, Y. Lee, S. Hong, J. Bae, J. An, Y. Kim, S. Cha, Int. J. Hydrogen Energy 40 (2015) 15704–15708.
[34] H. Choi, M. Kim, K. Neoh, D. Jang, H. Kim, J. Shin, G. Kim, J. Shim, Adv. Energy Mater 7 (2017) 1601956.
[35] Z. Duan, M. Yang, A. Yan, Z. Hou, Y. Dong, Y. Chong, M. Cheng, W. Yang, J. Power Sources 160 (2006) 57–64.
[36] W. Kim, H. Song, J. Moon, H. Lee, Solid State Ionics 177 (2006) 3211–3216.
[37] H. Shi, R. Ran, Z. Shao, Int. J. Hydrogen Energy 37 (2012) 1125–1132.

[38] H. Shi, G. Yang, Z. Liu, G. Zhang, R. Ran, Z. Shao, W. Zhou, W. Jin, Int. J. Hydrogen Energy 37 (2012) 13022–13029.
[39] G. Wang, Y. Zhang, M. Han, J. Electroanal. Chem. 857 (2020) 113591.
[40] H. Yahiro, K. Eguchi, H. Arai, Solid State Ionics 36 (1989) 71–75.
[41] K. Eguchi, T. Setoguchi, T. Inoue, H. Arai, Solid State Ionics 52 (1992) 165–172.
[42] D. Kim, J. Am. Ceram. Soc. 72 (1989) 1415–1521.
[43] Y. Kang, G. Choi, Solid State Ionics 180 (2009) 886–890.
[44] L. Villas-Boas, F. Figueiredo, D. Souza, F. Marques, Solid State Ionics 262 (2014) 522–525.
[45] Y. Zheng, M. Zhou, L. Ge, S. Li, H. Chen, L. Guo, J. Alloys Compd. 509 (2011) 546–550.
[46] S. Preethi, M. Abhiroop, K. Suresh Babu, Ceram. Int. 45 (2019) 5819–5828.
[47] J. Lane, J. Neff, G. Christie, Solid State Ionics 177 (2006) 1911–1915.
[48] T. Hsieh, D. Ray, Y. Fu, Ceram. Int. l39 (2013) 7967–7973.
[49] C. Madhuri, K. Venkataramana, A. Nurhayati, C. Reddy, Curr. Appl. Phys. 18 (2018) 1134–1142.
[50] K. Tanwar, N. Jaiswal, D. Kumar, O. Parkash, J. Alloys Compd. 684 (2016) 683–690.
[51] S. Acharya, V. Gaikwad, S. D'Souza, S. Barman, Solid State Ionics 260 (2014) 21–29.
[52] Y. Huang, A. Hussain, E. Wachsman, Nanomater. Energy 49 (2018) 186–192.
[53] Z. Shao, S. Haile, Nature 431 (2004) 170–173.
[54] X. Ding, Z. Gao, D. Ding, X. Zhao, H. Hou, S. Zhang, G. Yuan, Appl. Catal. B Environ. 243 (2019) 546–555.
[55] W. He, X. Wu, G. Yang, H. Shi, F. Dong, M. Ni, ACS Energy Lett 2 (2017) 301–305.
[56] Y. Zhang, J. Liu, X. Huang, Z. Lu, W. Su, Solid State Ionics 179 (2008) 250–255.
[57] X. Zhang, M. Robertson, C. Deċes-Petit, W. Qu, O. Kesler, R. Maric, D. Ghosh, J. Power Sources 164 (2007) 668–677.
[58] C. Su, Z. Shao, Y. Lin, Y. Wu, H. Wang, Phys. Chem. Chem. Phys. 14 (2012) 12173–12181.
[59] L. Zhao, B. He, J. Shen, F. Chen, C. Xia, Electrochem. Commun. 13 (2011) 450–453.
[60] W. Sun, Z. Shi, Z. Wang, W. Liu, J. Membr. Sci. 476 (2015) 394–398.
[61] H. Harwig, A. Gerards, J. Solid State Chem. 26 (1978) 265–274.
[62] J. Berezovsky, H. Liu, S. Dou, Solid State Ionics 66 (1993) 201–206.
[63] P. Shuk, H. Wiemhöfer, W. Göpel, Z. Anorg, Allg. Chem. 623 (1997) 892–896.
[64] N. Jiang, E. Wachsman, S. Jung, Solid State Ionics 150 (2002) 347–353.
[65] E. Orlova, E. Kharitonova, N. Gorshkov, V. Goffman, V. Voronkova, Solid State Ionics 302 (2017) 158–164.
[66] A. Yaremchenko, V. Kharton, E. Naumovich, A. Tonoyan, Mater. Res. Bull. 35 (2000) 515–520.
[67] Y. Ayhan, A. Buyukaksoy, Solid State Ionics 338 (2019) 66–73.
[68] D. Khaerudini, G. Guan, P. Zhang, X. Hao, A. Abudula, Rev. Chem. Eng. 30 (2014) 539–551.
[69] D. Khaerudini, G. Guan, P. Zhang, X. Hao, Y. Kasai, K. Kusakabe, A. Abudula, J. Alloys Compd. 589 (2014) 29–36.
[70] G. Paściak, J. Chmielowiec, S. Chan, Ceram. Int. 40 (2014) 8969–8974.
[71] W. Guo, J. Liu, J. Power Sources 195 (2010) 8185–8188.
[72] D. Joh, J. Park, D. Kim, B. Yun, K. Lee, J. Power Sources 320 (2016) 267–273.
[73] S. He, Q. Zhang, G. Maurizio, L. Catellani, K. Chen, Q. Chang, M. Santarelli, S. Jiang, ACS Appl. Mater. Interfaces 10 (2018) 40549–40559.
[74] T. Ishihara, H. Matsuda, Y. Takita, J. Am. Chem. Soc. 116 (1994) 3801–3803.
[75] T. Ishihara, H. Matsuda, Y. Takita, Solid State Ionics 79 (1995) 147–151.
[76] S. Yu, H. Bi, J. Sun, L. Zhu, H. Yu, C. Lu, X. Liu, J. Alloys Compd. 777 (2019) 244–251.
[77] T. Ishihara, J. Japan Pet. Inst 58 (2015) 71–78.
[78] K. Huang, J. Wan, J. Goodenough, J. Electrochem. Soc. 48 (2001) A788–A794.
[79] G. Yang, C. Su, R. Ran, M. Tade, Z. Shao, Energy Fuels 28 (2014) 356–362.
[80] Y. Huang, R. Dass, Z. Xing, J. Goodenough, Science 312 (2006) 254–257.
[81] B. Niu, C. Lu, W. Yi, S. Luo, X. Li, X. Zhong, X. Zhao, B. Xu, Appl. Catal. B Environ. 270 (2020) 118842.
[82] P. Singh, J. Goodenough, Energy Environ. Sci. 5 (2012) 9626–9631.
[83] P. Singh, J. Goodenough, J. Am. Chem. Soc. 135 (2013) 10149–10154.
[84] C. Tealdi, L. Malavasi, I. Uda, C. Ferrara, V. Berbenni, P. Mustarelli, Chem. Commun. 50 (2014) 14732–14735.
[85] I. Evans, J. Evans, H. Davies, A. Haworth, M. Tate, Chem. Mater. 26 (2014) 5187–5189.
[86] J. Xu, S. Liu, Q. Wang, J. Xiaofeng, X. Li, X. Kuang, J. Mater. Chem. A 4 (2016) 6313–6318.
[87] P. Chien, Y. Jee, C. Huang, R. Dervişoġlu, I. Hung, Z. Gan, K. Huang, Y. Hu, Chem. Sci. 7 (2016) 3667–3675.
[88] S. Fernández-Palacios, L. Santos-Gómez, J. Compana, J. Porras-Vázquez, A. Cabeza, D. Marrero-López, E. Losilla, Ceram. Int. 41 (2015) 6542–6551.
[89] K. Inglis, J. Corley, P. Florian, J. Cabana, R. Bayliss, F. Blanc, Chem. Mater. 28 (2016) 3850–3861.
[90] Y. Jee, X. Zhao, X. Lei, K. Huang, J. Am. Ceram. Soc. 99 (2016) 324–331.
[91] A. Pandey, U. Chanda, L. Besra, K. Sahu, A. Roy, S. Pati, J. Electroceram. 40 (2018) 50–56.
[92] D. Joh, H. Shin, J. Kim, K. Lee, J. Ind. Eng. Chem. 71 (2019) 387–392.
[93] E. Fabbri, L. Bi, H. Tanaka, D. Pergolesi, E. Traversa, Adv. Funct. Mater. 21 (2011) 158–166.
[94] H. Wang, X. Wang, B. Meng, X. Tan, K. Loh, J. Sunarso, S. Liu, J. Ind. Eng. Chem. 60 (2018) 297–306.
[95] K. Xie, R. Yan, X. Chen, D. Dong, S. Wang, X. Liu, G. Meng, J. Alloys Compd. 472 (2009) 551–555.
[96] A. Afif, N. Radenahmad, C. Lim, M. Petra, M. Islam, S. Rahman, S. Eriksson, A. Azad, Int. J. Hydrogen Energy 41 (2016) 11823–11831.
[97] T. Takahashi, H. Iwahara, Rev. Chim. Miner. 17 (1980) 243–253.
[98] H. Iwahara, T. Esaka, H. Uchida, N. Maeda, Solid State Ionics 3/4 (1981) 359–363.
[99] H. Iwahara, T. Esaka, H. Uchida, T. Yamauchi, K. Ogak, Solid State Ionics 18/19 (1986) 1003–1007.
[100] H. Iwahara, H. Uchida, K. Morimoto, J. Electrochem. Soc. 137 (1990) 462–465.
[101] T. Hibino, K. Mizutani, T. Yajima, H. Iwahara, Solid State Ionics 57 (1992) 303–306.
[102] H. Iwahara, T. Yajima, T. Hibino, K. Ozaki, H. Suzuki, Solid State Ionics 61 (1993) 65–69.
[103] G. Ma, T. Shimura, H. Iwahara, Solid State Ionics 110 (1998) 103–110.
[104] C. Duan, J. Huang, N. Sullivan, R. O'Hayre, Appl. Phys. Rev. 7 (2020), 011314.
[105] A. Lesnichyova, A. Stroeva, S. Belyakov, A. Farlenkov, N. Shevyrev, M. Plekhanov, I. Khromushin, T. Aksenova, M. Ananyev, A. Kuzmin, Materials 12 (2019) 2219.
[106] M. Wang, L. Qi, Chin. J. Chem. Phys. 21 (2008) 286–290.
[107] N. Matskevich, T. Wolf, M. Matskevich, T. Chupakhina, Eur. J. Inorg. Chem. (2009) 1477–1482, 2009.
[108] W. Wang, J. Liu, Y. Li, H. Wang, F. Zhang, G. Ma, Solid State Ionics 181 (2010) 667–671.
[109] N. Matskevich, T. Wolf, J. Chem. Thermodyn. 42 (2010) 225–228.
[110] J. Yin, X. Wang, J. Xu, H. Wang, F. Zhang, G. Ma, Solid State Ionics 185 (2011) 6–10.
[111] D. Medvedev, A. Murashkina, E. Pikalova, A. Demin, A. Podias, P. Tsiakaras, Prog. Mater. Sci. 60 (2014) 72–129.
[112] H. Matsumoto, Y. Kawasaki, N. Ito, M. Enoki, T. Ishihara, Electrochem. Solid ST 10 (2007) B77–B80.
[113] Y. Liu, R. Ran, S. Li, Y. Jiao, M. Tade, Z. Shao, J. Power Sources 257 (2014) 308–318.
[114] E. Shin, E. Anggia, J. Park, Solid State Ionics 339 (2019) 115007.
[115] L. Bi, S. Fang, Z. Tao, S. Zhang, R. Peng, W. Liu, J. Eur. Ceram. Soc. 29 (2009) 2567–2573.
[116] K. Katahira, Y. Kohchi, T. Shimura, H. Iwahara, Solid State Ionics 138 (2000) 91–98.
[117] K. Kreuer, S. Adams, W. Münch, A. Fuchs, U. Klock, J. Maier, Solid State Ionics 145 (2001) 295–306.
[118] J. Li, C. Wang, X. Wang, L. Bi, Electrochem. Commun. 112 (2020) 106672.
[119] R. Costa a, N. Grünbaum, M. Berger, L. Dessemond, A. Thorel, Solid State Ionics 180 (2009) 891–895.
[120] C. Peng, J. Melnik, J. Luo, A. Sanger, K. Chuang, Solid State Ionics 181 (2010) 1372–1377.
[121] A. Azad, S. Subramaniam, T. Dung, J. Alloys Compd. 334 (2002) 118–130.
[122] D. Gao, R. Guo, J. Alloys Compd. 493 (2010) 288–293.
[123] J. Tong, D. Clark, L. Bernau, M. Sanders, R. O'Hayre, J. Mater. Chem. 20 (2010) 6333–6341.
[124] C. Duan, J. Tong, M. Shang, S. Nikodemski, M. Sanders, S. Ricote, A. Almansoori, R. O'Hayre, Science 349 (2015) 1321–1326.
[125] J. Tong, D. Clark, M. Hoban, R. O'Hayre, Solid State Ionics 181 (2010) 496–503.
[126] D. Pergolesi, E. Fabbri, E. Traversa, Electrochem. Commun. 12 (2010) 977–980.
[127] J. Shim, J. Park, J. An, T. Gür, S. Kang, F. Prinz, Chem. Mater. 21 (2009) 3290–3296.
[128] K. Bae, D. Jang, H. Choi, D. Kim, J. Hong, B. Kim, J. Lee, J. Son, J. Shim, Nat. Commun. 8 (2017) 14533.
[129] Y. Liu, R. Ran, M. Tade, Z. Shao, J. Membr. Sci. 467 (2014) 100–108.
[130] Y. Guo, R. Ran, Z. Shao, Int. J. Hydrogen Energy 35 (2010) 5611–5620.
[131] W. Sun, M. Liu, W. Liu, Adv. Energy Mater 3 (2013) 1041–1050.
[132] Y. Liu, Y. Guo, R. Ran, Z. Shao, J. Membr. Sci. 415–416 (2012) 391–398.
[133] C. Zuo, S. Zha, M. Liu, M. Hatano, M. Uchiyama, Adv. Mater. 18 (2006) 3318–3320.
[134] L. Bi, Z. Tao, C. Liu, W. Sun, H. Wang, W. Liu, J. Membr. Sci. 336 (2009) 1–6.
[135] Y. Guo, Y. Lin, R. Ran, Z. Shao, J. Power Sources 193 (2009) 400–407.
[136] Y. Liu, Y. Guo, R. Ran, Z. Shao, J. Membr. Sci. 437 (2013) 189–195.
[137] K. Ryu, S. Haile, Solid State Ionics 125 (1999) 355–367.
[138] K. Xie, R. Yan, X. Liu, Electrochem. Commun. 11 (2009) 1618–1622.
[139] H. Wang, R. Peng, X. Wu, J. Hu, C. Xia, J. Am. Ceram. Soc. 92 (2009) 2623–2629.
[140] H. Iwahara, Solid State Ionics 52 (1992) 99–104.
[141] R. Peng, Y. Wu, L. Yang, Z. Mao, Solid State Ionics 177 (2006) 389–393.
[142] C. Zhou, J. Sunarso, Y. Song, J. Dai, J. Zhang, B. Gu, W. Zhou, Z. Shao, J. Mater. Chem. A 7 (2019) 13265–13274.
[143] B. Zhu, X. Liu, P. Zhou, X. Yang, Z. Zhu, W. Zhu, Electrochem. Commun. 3 (2001) 566–571.
[144] X. Wang, Y. Ma, S. Li, A. Kashyout, B. Zhu, M. Muhammed, J. Power Sources 196 (2011) 2754–2758.
[145] X. Wang, Y. Ma, R. Raza, M. Muhammed, B. Zhu, Electrochem. Commun. 10 (2008) 1617–1620.
[146] Y. Ma, X. Wang, S. Li, M. Toprak, B. Zhu, M. Muhammed, Adv. Mater. 22 (2010) 1640–1644.
[147] X. Wang, Y. Ma, B. Zhu, Int. J. Hydrogen Energy 37 (2012) 19417–19425.
[148] L. Fan, C. He, B. Zhu, Int. J. Energy Res. 41 (2017) 465–481.
[149] L. Fan, C. He, M. Chen, B. Zhu, J. Power Sources 234 (2013) 154–174.